This is the accepted manuscript made available via CHORUS. The article has been published as:

Local interactions in active matter are reinforced by spatial structure

Eighdi Aung, James E. McClure, and Nicole Abaid

Phys. Rev. E **110**, L062102 — Published 5 December 2024

DOI: 10.1103/PhysRevE.110.L062102

Local interactions in active matter are reinforced by spatial structure

Eighdi Aung
Engineering Mechanics Program, Virginia Tech, Blacksburg, Virginia, USA

James E. McClure
National Security Institute, Virginia Tech, Blacksburg, Virginia, USA

Nicole Abaid*
Department of Mathematics, Virginia Tech, Blacksburg, Virginia, USA
(Dated: November 7, 2024)

The flocking of self-propelled particles in heterogeneous environments is relevant to both natural and artificial systems. The Vicsek model is a canonical choice to investigate such systems due to the minimal number of parameters required to define flocking. Prior research on the Vicsek model has investigated the effects of interaction rules, particle speed, and obstacle packing on the flocking behavior, but the effect of interaction radius remains an open question. Unlike obstacle-free domains, the locality of interactions not only affects how quickly the system can become polarized, but also how well the flocks can align or realign after colliding with obstacles. In this letter, we delve into this subtle relationship that exists in the scale of the perception of Vicsek particles in the presence of obstacles. We demonstrate that the presence of obstacles impacts group density, which provides the basis to identify distinct phases for collective behavior. This leads to the counter-intuitive result that obstacles, while generally confounding for macroscopic order, may enable global order even as noise in the system increases.

Active matter comprises a broad class of physical systems defined by emergent collective behaviour, ranging from bird flocks and human crowds to the dynamic interactions of bacteria and tissues. In contrast with standard diffusion processes described by Brownian motion, self-propelled particles can align their motion to cover distance more efficiently. The associated scaling behavior of mean square displacement with time is thereby super-diffusive [1]. This tendency is confounded by the presence of obstacles, since confinement produces a sub-diffusive effect [2, 3]. It follows that active matter is subject to competing effects within confined environments. How well groups of self-propelled particles can coordinate their motion in an environment constrained by structure is a compelling topic due to the existence of natural [4–7] and artificial [8, 9] systems that perform flocking in the presence of obstacles. The essence of flocking in such environments relies on the interplay of interactions among particles, as well as their response to the constraints the environment imposes on their movement. We demonstrate that the presence of obstacles alters the dominant polarization regimes for active matter, and that these regimes are controlled by the ratio of the length scale for interactions relative to the size of the structures. Obstacles can also lead to the formation of more tightly packed flocks, such that structural heterogeneity within the system is reinforced as a consequence of this interaction.

The canonical Vicsek model [10, 11] generates flocking using a minimal amount of parameters to define the dynamics. Many variations of the Vicsek model have been explored [1, 12–17]. In recent years, the behavior of the Vicsek model in environments with obstacles has been examined. Martinez et al. [18] performed a comprehensive study of such a system by investigating how much coordination is achievable according to the type of collision rules imposed, the particle speed, and the obstacle packing fraction. Rahmani et al. [19] extended the study of the Vicsek model with obstacles by using topological interaction rules and showed that, even for metric-free interactions, flocking arises due to spatial heterogeneity and is density dependent. Furthermore, Codina et al. [20] showed that a single minuscule obstacle can produce flock reversal of Vicsek particles. Most recently, Serna et al. [21] identified the existence of phases in the scale of flocking in a Vicsek system as a function of the spacing between obstacles in the environment.

To further the understanding of the Vicsek system with obstacles, we focus on the effect of the interaction radius on flocking. The key feature of the Vicsek model is the ability of the system to self-organize into flocks from local interactions. In an obstacle-free domain, the extent to which the system is "local", i.e., the interaction radius is smaller than the domain size, would naturally be defined by the particular biological or physical system we are investigating. For example, to model a bird flock, we would use the visual range to define the particles' interaction radius. In the case of low noise in such a system, we can expect that the interaction radius would only affect how quickly the system can reach global polarization. However, the same cannot be said for a Vicsek system with obstacles because, even in the absence of noise, the system will never sustain global polarization. Even more so, the system may have multiple steady-states for which global polarization may occur. Hence, in heterogeneous environments, the locality of in-

* nabaid@vt.edu

teraction impacts the flock's ability to retain alignment or realign after colliding with obstacles. In this letter, we explore this nuanced relationship between the scale of a particle's perception and quenched disorder that exists in a system with obstacles. Specifically, we show the existence of different phases of flocking due to the coupling that exists between the particle's interaction range and the size of the obstacles in the environment.

We use the 2D Vicsek model [10] with N particles in a periodic box of length L. The i^{th} particle at timestep t has position $\mathbf{x}_i(t) \in [-L/2, L/2]^2$ and velocity $\mathbf{v}_i(t) \in \mathbb{R}^2$. At each timestep, particle i heads in the direction $\theta_i(t) = \arg[\mathbf{v}_i(t)] \in [-\pi, \pi]$. A particle's heading updates by averaging the heading of neighboring particles within an interaction radius, R, subject to noise, ξ, which is sampled uniformly from $[-\pi, \pi]$ with strength η. Thus, the heading update of the i^{th} particle with neighbors indexed j is:

$$\theta_i(t + \Delta t) = \langle \theta_j(t) \rangle_R + \eta\, \xi, \tag{1}$$

The particle then updates its velocity and position:

$$\mathbf{v}_i(t + \Delta t) = \cos[\theta_i(t + \Delta t)]\mathbf{e}_1 + \sin[\theta_i(t + \Delta t)]\mathbf{e}_2, \tag{2}$$
$$\mathbf{x}_i(t + \Delta t) = \mathbf{x}_i(t) + c\, \mathbf{v}_i(t + \Delta t), \tag{3}$$

where $\mathbf{e}_1$ and $\mathbf{e}_2$ are unitary basis vectors of $\mathbb{R}^2$, and c is the constant speed of the particle. With the addition of obstacles to the domain, we add the condition that, if the updated position of the particle is inside an obstacle, then the particle performs an avoidance maneuver on heading while remaining fixed for that timestep:

$$\mathbf{v}_i(t + \Delta t) = \mathbf{v}_i(t) \times \beta\, \mathbf{e}_3, \tag{4}$$
$$\mathbf{x}_i(t + \Delta t) = \mathbf{x}_i(t), \tag{5}$$

where β is a binomial random choice between $\{-1, 1\}$ multiplying the unitary vector $\mathbf{e}_3 = \mathbf{e}_1 \times \mathbf{e}_2$ with $\mathbf{v}_i(t)$, $\mathbf{e}_1$, and $\mathbf{e}_2$ nominally extended to three dimensions to perform the cross product. We choose to model obstacle avoidance in this way to allow the particle to make an unbiased choice between turning left or right orthogonally to their previous heading. The obstacles in this model are treated as solid objects so that the particles cannot sense through them. Please see Section I of Supplemental Material [22] for exploration on the effect of transparent obstacles. We also want to note that the particles are point-masses and there is no volume exclusion rule in the model.

Figure 1A shows a snapshot of a canonical Vicsek system. As shown in Figure 1B, we designed the domain to have two rows of three obstacles. We spaced the obstacles equidistantly from the boundaries horizontally and vertically such that, $\delta_c = \delta_{c_1} + \delta_{c_2}$ and $\delta_r = \delta_{r_1} + \delta_{r_2}$, respectively. For this study, the periodic box has length $L = 5$ and the obstacles have $R_o = 0.4$, making $\delta_r = 1.70$ and $\delta_c = 0.87$. The density, ρ, is the ratio of the total number of particles, N, to the unobstructed area; we set $\rho = 20$ which means $N = 500$ without obstacles and

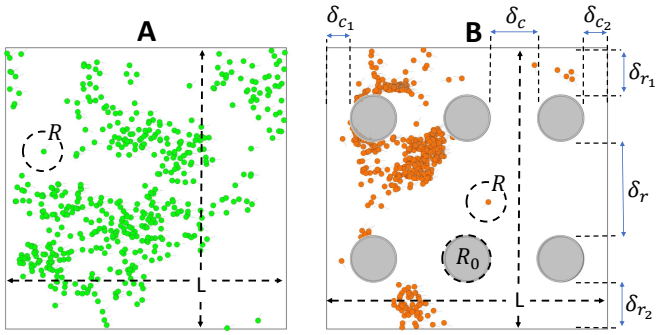


FIG. 1. Snapshot of Vicsek particles (A) without and (B) with obstacles with interaction radius $R = 0.28$ and $\eta = 0.12$, confined in periodic boxes with $L = 5$. The grey circles in figure B indicate obstacles with radius $R_o = 0.4$. The obstacles are equidistantly arranged with horizontal and vertical gap spacings δ_c and δ_r. To ensure equal spacing around the periodic boundaries, $\delta_{c_1} + \delta_{c_2} = \delta_c$ and $\delta_{r_1} + \delta_{r_2} = \delta_r$.

$N = 440$ with obstacles. We fix the speed to be $c = 0.05$, so that particles need on the order of 100 timesteps to traverse the domain with $\Delta t = 1$. Hence, we only vary R and η.

For a Vicsek system without obstacles, the interaction radius is naturally bounded above by L. On the other hand, with obstacles, the interaction between particles is also influenced by obstacle size, which has $R_o << L$. We propose a characteristic radius, r, to be the ratio of the interaction radius to the obstacle size. For this study, we focus on $\eta \in [0, 0.5]$ and $r = R/R_o \in [0.1, 6.25]$. For each choice of noise and interaction radius, we run 100 Monte Carlo simulations of 10,000 timesteps with random initial conditions.

In the Vicsek model, the inter-particle interaction is defined as heading alignment. Hence, the natural choice for an order parameter is polarization, which is the magnitude of the sum of the particles' velocities normalized by particle number and constant speed. We compute the steady-state mean polarization over T timesteps:

$$\varphi = \left\langle \frac{1}{N} \left\| \sum_{i=1}^{N} \mathbf{v}_i(t) \right\| \right\rangle_T. \tag{6}$$

We define steady-state to be when there is no significant change in the mean and variance of the order parameter, which is reached after 2000 timesteps, making $T = 8000$.

We first explore how polarization changes with noise and interaction radius when obstacles are present. We expect that polarization will be strictly less than one (i.e, $\varphi < 1$), even in the absence of noise (i.e, $\eta = 0$), since particles are sure to encounter obstacles and disperse frequently. Furthermore, recent literature [18, 23] has shown that, at low noises, polarization as a function of noise exhibits non-monotonicity in contrast with the Vicsek model without obstacles. The non-monotonic behavior is driven by the particles' collisions with obstacles and noise. Figure 2 shows example cases of polarization

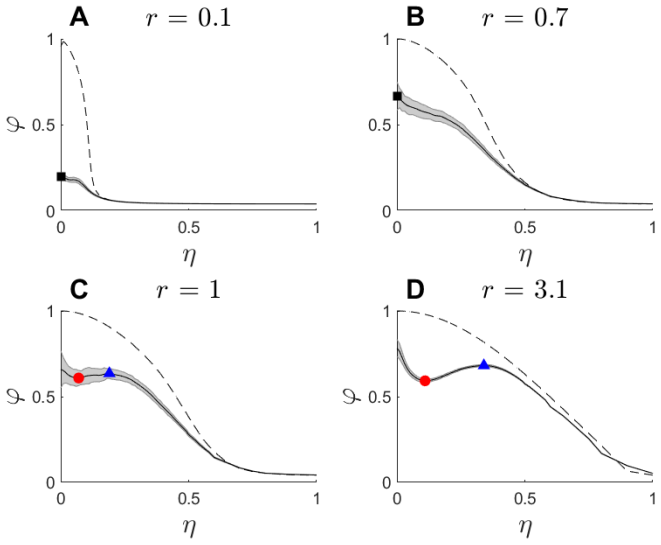


FIG. 2. Mean polarization over $T = 8000$ timesteps, as a function of noise, η, for example cases of the characteristic radius, r. Curves indicate the mean polarization over 100 Monte Carlo replicates and shaded regions show $\pm$ one standard deviation. The black square markers indicate the location of global maxima when the curves do not have critical points. This behavior is observed in figures A and B, which have interaction radii less than the radius of the obstacles, i.e., $r < 1$. When $r \geq 1$, local extrema appear. The local minimum and maximum are marked by red circles and blue triangles, respectively, shown in figures C and D. The dashed lines show the polarization curves obtained for a Vicsek system without obstacles using $R = 0.4r$ with the value of r in each figure title.

as a function of noise for increasing values of interaction radius. The top plots, for which $R < R_o$, do not have the characteristic concavity of the polarization plots for the Vicsek model without obstacles. They also attain much lower maximum values of polarization by comparison. Interestingly, the bottom plots, for which $R \geq R_o$, show the appearance of local extrema of the polarization curves. The order in which the local minimum and maximum points appear is directly tied to noise. At low noise, the system consists of tightly packed flocks, as opposed to a noisier system where the flocks are dispersed. The dispersal of flocks due to noise compensates for the reduction in polarization due to collisions with obstacles, consistent with [24]. Additionally, we observe that increasing interaction radius widens the spacing between the two critical points.

Figures 3A and C show heatmaps of φ, denoted on the coloraxis, as a function of r and η. We observe two general regimes of polarization in both figures, however we do not see high polarization values ($\varphi > 0.6$) in the presence of obstacles. We find the two level curves of highest curvature in the heatmaps, $\varphi = \{0.18, 0.74\}$ and $\varphi = \{0.12, 0.60\}$, for the Vicsek system with and without obstacles, respectively, following the procedure detailed in Section III of Supplemental Material [22]. The level curves separate low, intermediate, and high polarization regimes in the parameter space. For all values of η, horizontal slices in Figure 3A show a monotonic increase, as expected of a Vicsek system without obstacles. We see similar behavior, although only lower polarization values are attained, when obstacles are present and $\eta > 0.1$ in Figure 3C.

In stark contrast, for $\eta \leq 0.1$ with obstacles, we observe the reappearance of the intermediate regime in the lower-right corner, meaning that polarization attains a maximum value for fixed noise at some intermediate value of r. This feature is directly tied to the existence of local critical points in the polarization curves when the obstacles are present. As seen from the polarization curves, Figure 2C and D, the existence of local maximum and minimum polarizations for values of $r \geq 1$ depends solely on η. Therefore, we require an additional order parameter that can decouple the effects of r and η. From observing the system dynamics, we determine that spatial coverage is a reasonable and simple choice to parameterize the effect of η. We quantify coverage, σ, as the steady-state time averaged fraction of area occupied by particles:

$$\sigma = \left\langle \frac{b_o(t)}{b} \right\rangle_T, \tag{7}$$

where we discretize the domain into $b = 100$ total bins and $b_o(t)$ is the number of bins occupied by particles at time t. Figures 3B and D are the heatmaps of coverage for systems without and with obstacles, respectively. The level curves obtained from the polarization heatmaps are overlaid on the coverage heatmaps. The sensitivity of coverage to noise is strikingly evident from vertical stacking of prominent regimes in the parameter space.

The polarization heatmap is used to define dynamical phases that the Vicsek system exhibits in parameter space, while the coverage heatmap is used to elucidate the role of flock density on phase transitions. Figure 3B is labeled with the observed phases bounded by level curves of polarization and overlaid on the heatmap of coverage values. We identify phase (I) where the system is weakly polarized and the particles are moving in different directions. In this phase, the system is qualitatively gaseous. Either increasing interaction radius or decreasing noise brings the system to a transition phase, (II), where it starts to form local order but does not have consistently cohesive flocks due to retaining randomness from the gaseous phase. Decreasing the noise η generally brings the system to a highly polarized phase, (III). We can qualitatively define this highly polarized phase to be liquid-like, where macroscopic flow in the flock is observed. This is a known feature in a typical Vicsek system. From observing the coverage heatmap, we can see that the variation in coverage values are predominantly in the highly polarized phase. This shows that a Vicsek system can reach consensus as long as it is allowed to evolve over enough time irrespective of particle density, suggesting that the "locality" of interactions in a Vicsek system without obstacles is only bounded below by

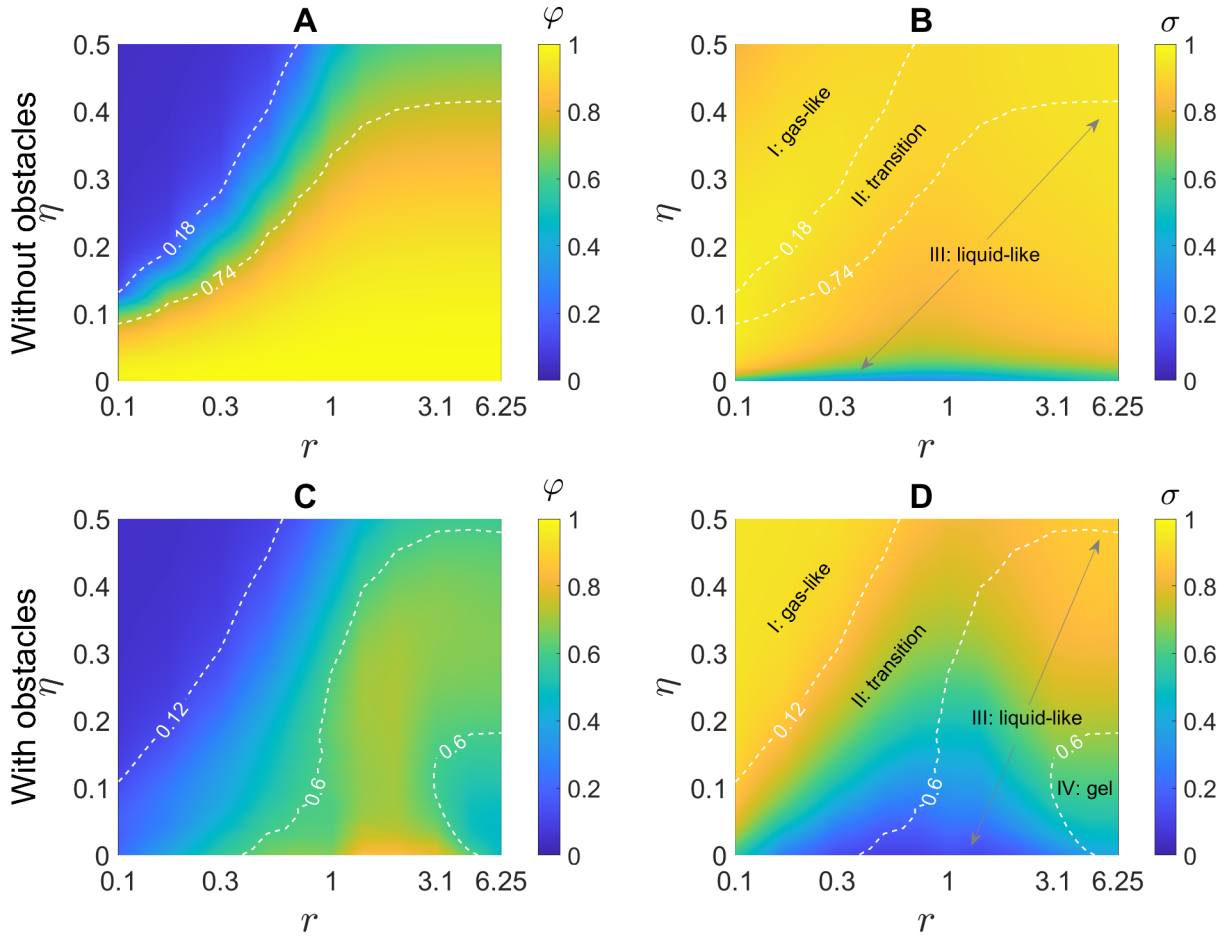


FIG. 3. Polarization (A) and coverage (B) heatmaps for the Vicsek system without obstacles in the parameter space of η and r, with phases labeled on B. Figures C and D show the same quantities for the Vicsek system with obstacles. The horizontal axes for all the figures are use a logarithmic scale. We observed three main regimes of polarization which we identify from drawing contours of $\varphi = \{0.18, 0.74\}$ for figure A and $\varphi = \{0.12, 0.60\}$ for figure B. The contours of polarization are overlaid on the coverage heatmaps shown in figures B and D. Phase (I) is weakly polarized and no general flocking motion can be observed, hence, gas-like. Flocks start to form in the transition phase (II). Highly polarized flocks are observed in phase (III). In Phase (IV), only observed when obstacles are present, the system exhibits high synchronicity for the exchange of low polarization.

$r = 0$. In other words, the Vicsek system in the absence of obstacles can obtain the highly polarized phase as long as there exists a non-zero interaction radius.

We identify similar phases for a Vicsek system with obstacles, though the presence of obstacles noticeably affects the phases shown in Figure 3D. The first noticeable change is in the growth of the transition phase, overtaking the liquid-like phase. This effect is intuitive since we already know that obstacles introduce more disorder in the system. Interestingly, the liquid-like phase no longer starts at bottom left corner of Figure 3D, indicating that there is a non-zero lower bound for the interaction radius. We also observe that the variation in the coverage heatmap now extends into the transition phase, suggesting a stronger influence of particle density on the phase transition of flocking behavior in the presence of obstacles. Specifically, we observe a diagonal variation in coverage values in the transition region, as opposed to a vertical-stacking variation in the liquid-like region. Interestingly, Figure 3C shows the reappearance of the intermediate polarization phase for $r > 3.1$, which we qualitatively characterize as the gel-like phase, phase (IV). The existence of this phase ties to the non-monotonic behavior of the polarization curves, see Figure 2D. In this phase, the system quickly reaches alignment such that the particles move in synchrony in a rigidly locked state. When any part of the group encounters an obstacle in this interlocked state, the entire group responds, causing particles to experience "virtual" obstacles even when they are in open space. We find a stronger influence of this behavior if the particles are able to sense through the obstacles, resulting in lower polarization in the liquid-like phase and the slight growth of the gel phase (see Section I of Supplemental Material [22]). In the gel phase, the flocks behave like a viscous liquid which temporarily "sticks" to the obstacles due to the inertia created from

responding to large interaction radius. The sticking is directly caused by the interaction term dominating the obstacle maneuver consistently over time for dispersed flocks. We note that this interlocked flocking phase is latent in Figure 3C, but is indistinguishable from the rest of the yellow phase due to the absence of obstacles. In the context of a larger system size, we find that the extent of the gel phase shrinks in parameter space due to increasing the number of obstacles, as shown in Section II of Supplemental Material [22]. While one may expect the convergence of the phase diagram when studying finite-size effects, it should also be noted that self-averaging behavior can be lost whenever quenched disorder, obstacles in our case, is introduced in the system [25].

In summary, we observed that the interaction radius profoundly affects the behavior of the Vicsek system, and even more so, that such an effect is most prevalent in the presence of obstacles. Analogous to a thermodynamic system, the noise acts like temperature and the interaction radius acts like intermolecular bonding for the flocks. As such, we generally find that increasing noise (i.e., moving rightwards in subplots of Figure 3) in the phase space leads to states of higher entropy, and increasing interaction radius (i.e., moving upwards in subplots of Figure 3) in the phase space leads to states of lower entropy. The latter trend is more striking in the presence of obstacles, which implies that the "locality" in the interactions matters more when space is constrained. Additionally, we see that a non-zero minimal interaction radius is required to achieve substantial flocking in the system. Most interestingly, in the presence of obstacles, noise and interaction radius effect the system counterintuitively based on what we know about Vicsek flocks in open domains. When obstacles are present, higher noise may lead to higher order rather than disorder, and a larger sensing range can cause more frustration to order in the system, rather than enabling coordination among the particles.

ACKNOWLEDGMENTS

This work was supported by the National Science Foundation under award 1751498. The authors are grateful to Advanced Research Computing at Virginia Tech for computing resources.

[1] H. Chaté, F. Ginelli, G. Grégoire, F. Peruani, and F. Raynaud, Modeling collective motion: variations on the vicsek model, The European Physical Journal B **64**, 451 (2008).
[2] T. Neusius, I. M. Sokolov, and J. C. Smith, Subdiffusion in time-averaged, confined random walks, Physical Review E **80**, 011109 (2009).
[3] S. Condamin, O. Bénichou, and J. Klafter, First-passage time distributions for subdiffusion in confined geometry, Physical Review Letters **98**, 250602 (2007).
[4] L. Cisneros, C. Dombrowski, R. E. Goldstein, and J. O. Kessler, Reversal of bacterial locomotion at an obstacle, Physical Review E **73**, 030901 (2006).
[5] S. Battersby, The cells that flock together, Proceedings of the National Academy of Sciences **112**, 7883 (2015).
[6] D. J. Evangelista, D. D. Ray, S. K. Raja, and T. L. Hedrick, Three-dimensional trajectories and network analyses of group behaviour within chimney swift flocks during approaches to the roost, Proceedings of the Royal Society B: Biological Sciences **284**, 20162602 (2017).
[7] L. Ning, X. Lou, Q. Ma, Y. Yang, N. Luo, K. Chen, F. Meng, X. Zhou, M. Yang, and Y. Peng, Hydrodynamics-induced long-range attraction between plates in bacterial suspensions, Physical Review Letters **131**, 158301 (2023).
[8] F. Gökçe and E. Şahin, The pros and cons of flocking in the long-range "migration" of mobile robot swarms, Theoretical Computer Science **411**, 2140 (2010).
[9] L. Varga, A. Libál, C. Reichhardt, and C. Reichhardt, Pattern formation and flocking for particles near the jamming transition on resource gradient substrates, Physical Review E **106**, 064602 (2022).
[10] T. Vicsek, A. Czirók, E. Ben-Jacob, I. Cohen, and O. Shochet, Novel type of phase transition in a system of self-driven particles, Physical Review Letters **75**, 1226 (1995).
[11] F. Ginelli, The physics of the Vicsek model, European Physics Journal Special Topics **225**, 2099 (2016).
[12] G. Grégoire and H. Chaté, Onset of collective and cohesive motion, Physical Review Letters **92**, 025702 (2004).
[13] P. Degond and S. Motsch, Continuum limit of self-driven particles with orientation interaction, Mathematical Models and Methods in Applied Sciences **18**, 1193 (2008).
[14] J. Zhang, Y. Zhao, B. Tian, L. Peng, H.-T. Zhang, B.-H. Wang, and T. Zhou, Accelerating consensus of self-driven swarm via adaptive speed, Physica A: Statistical Mechanics and its Applications **388**, 1237 (2009).
[15] A. W. Baggaley, Model flocks in a steady vortical flow, Physical Review E **91**, 053019 (2015).
[16] A. Costanzo, E. van Haeringen, and C. Hemelrijk, Effect of time-delayed interactions on milling: A minimal model, Europhysics Letters **138**, 22002 (2022).
[17] S. Chatterjee, M. Mangeat, C.-U. Woo, H. Rieger, and J. D. Noh, Flocking of two unfriendly species: The two-species vicsek model, Physical Review E **107**, 024607 (2023).
[18] R. Martinez, F. Alarcon, D. R. Rodriguez, J. L. Aragones, and C. Valeriani, Collective behavior of vicsek particles without and with obstacles, The European Physical Journal E **41**, 1 (2018).
[19] P. Rahmani, F. Peruani, and P. Romanczuk, Topological flocking models in spatially heterogeneous environments, Communications Physics **4**, 206 (2021).
[20] J. Codina, B. Mahault, H. Chaté, J. Dobnikar, I. Pagonabarraga, and X.-q. Shi, Small obstacle in a large polar flock, Physical Review Letters **128**, 218001 (2022).
[21] H. Serna and W. T. Góźdź, The influence of obstacles on

the collective motion of self-propelled objects, Physica A: Statistical Mechanics and its Applications **625**, 129042 (2023).

[22] See Supplemental Material at [URL] for sections (I) the effect of transparent obstacles; (II) the effect of increasing system size; and (III) the method for finding transition level curves. Supplemental Material also contains reference [26].

[23] J. E. McClure and N. Abaid, Effect of topology and geometric structure on collective motion in the vicsek model, Frontiers in Applied Mathematics and Statistics **8**, 829005 (2022).

[24] O. Chepizhko, E. G. Altmann, and F. Peruani, Optimal noise maximizes collective motion in heterogeneous media, Physical Review Letters **110**, 238101 (2013).

[25] Y. Duan, B. Mahault, Y.-q. Ma, X.-q. Shi, and H. Chaté, Breakdown of ergodicity and self-averaging in polar flocks with quenched disorder, Physical Review Letters **126**, 178001 (2021).

[26] J.-C. Léger, Menger curvature and rectifiability, Annals of Mathematics **149**, 831 (1999).